Acta Crystallographica Section B
**Structural Science**
ISSN 0108-7681

# Bulk modulus and non-uniform compression of $Nb_3Te_4$ and $In_xNb_3Te_4$ ($x < 1$) channel compounds

**Markus Wunschel,[a] Robert E. Dinnebier,[a] Stefan Carlson[b]† and Sander van Smaalen[a]***

[a]Laboratory of Crystallography, University of Bayreuth, D-95440 Bayreuth, Germany, and [b]High Pressure Group, ESRF, BP 220, F-38043 Grenoble CEDEX, France

† Current address: MAX-lab, Lund University, PO Box 118, SE-221 00 Lund, Sweden.

Correspondence e-mail: smash@uni-bayreuth.de

Received 29 March 2001
Accepted 11 July 2001

The crystal structures of $Nb_3Te_4$ and $In_xNb_3Te_4$ [$x = 0.539$ (4)] are reported for a series of pressures between 0 and 40 GPa. Both compounds crystallize in space group $P6_3/m$ with $a = b = 10.671$ and $c = 3.6468$ Å for $Nb_3Te_4$, and $a = b = 10.677$ and $c = 3.6566$ Å for $In_xNb_3Te_4$ at ambient conditions. Phase transitions were not observed. High-pressure X-ray powder diffraction was measured using a diamond anvil cell and synchrotron radiation. Full Rietveld refinements provided the values of the lattice parameters and the values of the atomic coordinates at each pressure. The bulk modulus is found as $K_0 = 70$ (5) GPa for $Nb_3Te_4$ and as $K_0 = 73$ (4) GPa for $In_xNb_3Te_4$. The analysis of the pressure dependences of the detailed crystal structures shows that the compression along **c** involves the folding up of the quasi-one-dimensional zigzag chains of Nb. The compression perpendicular to **c** is entirely due to the reduction of the diameter of the channels. The presence of intercalated In atoms is found to have hardly any influence on the compression behaviour up to 40 GPa.

## 1. Introduction

The transition-metal chalchogenide triniobium tetratelluride ($Nb_3Te_4$) was first synthesized by Selte & Kjekshus (1964). $Nb_3Te_4$ is interesting because it has a quasi-one-dimensional (one-dimensional) crystal structure and it displays the properties of a one-dimensional electron band.

At ambient conditions $Nb_3Te_4$ has a hexagonal crystal structure, with space group $P6_3/m$ and lattice parameters $a = b = 10.671$ and $c = 3.6468$ Å (Fig. 1; Selte & Kjekshus, 1964). Two one-dimensional features can be recognized. Firstly, channels exist centered on the sixfold screw axes, which are bounded by Te atoms, and that are wide enough to accommodate additional atoms (Huan & Greenblatt, 1987). Despite this large empty space, the crystal structure of $Nb_3Te_4$ is stable and it remains so up to pressures of 40 GPa, as shown by the present experiments.

Secondly, the structure contains zigzag chains of Nb atoms parallel to the hexagonal axis. Along the chains the Nb—Nb distance ($d = 2.97$ Å) is only slightly larger than the corresponding distance in niobium metal ($d = 2.86$ Å; Villars & Calvert, 1996), whereas between chains Nb atoms are at least 3.85 Å apart. The chains support a one-dimensional electron band and they are considered to be responsible for the one-dimensional electronic properties of $Nb_3Te_4$ (Oshiyama, 1983).

The electrical conductivity of $Nb_3X_4$, with $X$ = S, Se, Te, is anisotropic with *e.g.* $\sigma_c$:$\sigma_a$ = 15:1 for the compound $Nb_3S_4$ (Ishihara & Nakada, 1982). In $Nb_3Te_4$ a commensurate charge-density wave (CDW) develops below $T_{CDW} = 80$ K, as

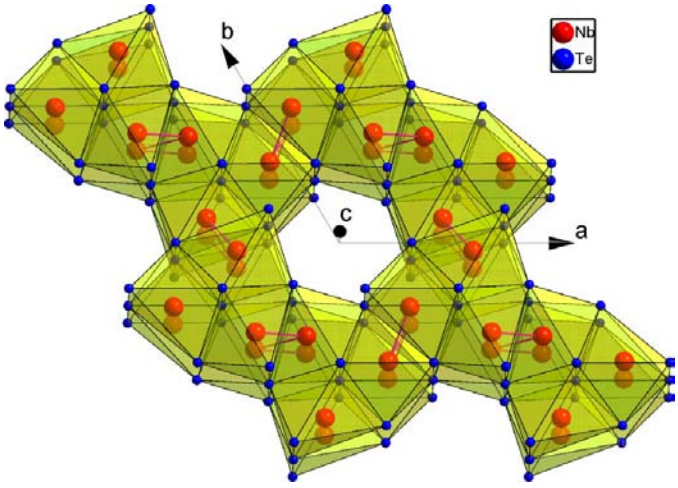


**Figure 1**
Crystal structure of $Nb_3Te_4$. 2 * 2 * 2 unit cells are displayed.

is evidenced by an anomaly in the electrical resistivity (Ishihara & Nakada, 1983) and by the observation of satellite reflections in X-ray scattering below $T_{CDW}$ at positions given by $\mathbf{q} = \pm(\frac{1}{3}\mathbf{a}^* + \frac{1}{3}\mathbf{b}^*) + \frac{3}{7}\mathbf{c}^*$ (Sekine *et al.*, 1987).

Different metal atoms can be intercalated into the channels, resulting in compounds $M_xNb_3Te_4$ with $0 < x \leq 1$ and $M$ = In, Tl, Na,... (Huan & Greenblatt, 1987). The maximum value of $x$ depends on the valence of $M$, such that a maximum of 1 electron per formula unit is transferred from $M$ to the $Nb_3Te_4$ framework. The CDW transition is preserved upon intercalation, but its characteristics are changed. For $In_xNb_3Te_4$ it was shown that $T_{CDW}$ increases with increasing $x$. Furthermore, the CDW is incommensurate along $c^*$ for $x > 0.4$, except for $x = 0.75$, where it is again commensurate (Othani *et al.*, 1993; Othani *et al.*, 1999; Boswell & Bennet, 1996).

In this work we concentrate on the structural quasi-one-dimensionality. X-ray powder diffraction is used to study the compression behavior of $Nb_3Te_4$ and $In_xNb_3Te_4$ ($x$ = 0.54). Rietveld refinements at a series of pressures allows us to determine the equations of state (EOSs) of both compounds, as well as the dependences of the crystal structures on pressure. Both compounds are found to be stable up to pressures of 40 GPa. The compression is found to correspond mainly to a reduction of the diameters of the channels. At first glance, surprisingly, we find that intercalation of indium hardly affects the compression behavior.

## 2. High-energy X-ray diffraction

$Nb_3Te_4$ was synthesized following the procedure in Huan & Greenblatt (1987). About 1 g of a stoichiometrical mixture of the elements was sealed in evacuated quartz tubes. The tubes were heated with 40 K $h^{-1}$ to 1273 K. After 10 d they were cooled down to room temperature at $-40$ K $h^{-1}$.

Compounds $In_xNb_3Te_4$ were prepared by mixing indium metal with finely ground previously synthesized $Nb_3Te_4$. Mixtures with various $x$ were sealed in evacuated quartz tubes and heated to 873 K with 50 K $h^{-1}$. After 3 weeks the samples were slowly cooled to room temperature with $-25$ K $h^{-1}$. Samples were ground and used in the diffraction measurements without further treatment.

High-pressure X-ray scattering experiments were performed on $Nb_3Te_4$ and on $In_xNb_3Te_4$ with the nominal composition $x = 0.75$. The value of $x$ was determined in a seperate diffraction experiment at the insertion device high-energy beamline ID15B of the European Synchrotron Radiation Facility (ESRF) in Grenoble, France. X-rays of energy 89 keV were selected by a bent Si (511) monochromator, which focuses the beam in the horizontal plane (Suortti *et al.*, 2001). The size of the beam was adjusted to a height and width of 0.2 mm. Details of the experimental setup are described in the beamline handbook. As detector, a Marresearch MAR345 image-plate reader was used at a distance of 717 mm from the sample. The wavelength was determined to 0.13918 Å from a Molybdenum standard. The samples were contained in 0.5 mm lithiumborate glass (glass No. 50) capillaries and were rocked for several degrees during measurements in order to improve randomization of the crystallites. An exposure time of 360 s was chosen. Data reduction was performed using the program *FIT2D* (Hammersley *et al.*, 1998), resulting in diagrams of corrected intensities *versus* the scattering angle $2\theta$. It was observed that the diffracted intensity was quite uniformly distributed over the Debeye–Scherrer rings, ruling out severe grain size effects. Low-angle diffraction peaks had a FWHM of 0.034° $2\theta$, which can be considered as the highest resolution for this particular setup.

Using very high energy for powder diffraction experiments enables the use of transmission geometries for strongly absorbing samples. This reduces grain size and the preferred orientation effects. Also the overspill effect, a common problem in flat-plate reflection experiments, is not present for a transmission setup. This reduces systematic errors in the measured intensities and structure factors and leads to *e.g.* more accurate difference-Fourier plots. For $Nb_3Te_4$ and $In_xNb_3Te_4$ the linear absorption coefficients are approximately 120 times smaller at a wavelength of 0.14 Å compared with the values for Cu $K\alpha_1$ radiation.

Starting with the known values of the lattice parameters of pure $Nb_3Te_4$ a Le Bail fit was produced in order to determine the lattice parameters and peak profile functions. The peak profile was described by a pseudo-Voigt function, together with an empirical function for the correction of the small asymmetry of the peaks. The background was described as the sum of a manual background and a four-term Legendre polynomial. The final fit revealed eight small additional maxima, which were not described by the hexagonal lattice. We believe that these maxima are Bragg reflections of impurity phases, but they could not be assigned to any particular compound. $2\theta$ regions around the positions of each of these impurity peaks were excluded from all subsequent refinements.

Initial Rietveld refinements were performed with the lattice-, profile- and background parameters fixed at their values obtained by the Le Bail fit. Starting coordinates of

**Table 1**
Lattice and profile parameters for the final Rietveld refinement of the high-energy data of $In_xNb_3Te_4$.

| | |
|---|---|
| Space group | $P6_3/m$ |
| $a = b$ (Å) | 10.6768 (3) |
| $c$ (Å) | 3.6566 (1) |
| Zeroshift | 0.60 (2) |
| *BG*1 | −38 (2) |
| *BG*2 | −31 (3) |
| *BG*3 | 10 (3) |
| *BG*4 | −36 (3) |
| *GP* | 1.31 (2) |
| *LX* | 0.63 (3) |
| *LY* | 12.4 (6) |
| Asymmetry | −0.029 (2) |
| $R_p$ | 0.026 |
| $R_{wp}$ | 0.042 |
| $R_{Bragg}$ | 0.043 |

**Table 2**
Structural parameters of $Nb_3Te_4$ at selected pressures ($P$).

Nb is at ($x$, $y$, $\frac{1}{4}$), Te1 is at (2/3, 1/3, $\frac{1}{4}$) and Te2 is at ($x$, $y$, $\frac{1}{4}$).

| Parameter | $P$ = 0.4 GPa | $P$ = 30.8 GPa |
|---|---|---|
| $a$ (Å) | 10.6338 (3) | 9.931 (3) |
| $c$ (Å) | 3.6371 (1) | 3.3886 (9) |
| $x$(Nb) | 0.4888 (4) | 0.483 (1) |
| $y$(Nb) | 0.1067 (4) | 0.107 (1) |
| $x$(Te2) | 0.3296 (4) | 0.3085 (7) |
| $y$(Te2) | 0.2697 (3) | 0.2493 (8) |
| $U_{iso}$ | 0.0002 (5) | 0.017 (1) |

niobium and tellurium were obtained from the known structure of $Nb_3Te_4$ (Selte & Kjekshus, 1964). The refinement converged to a good fit with $R_p = 0.112$ and $R_{Bragg} = 0.110$. A difference-Fourier revealed additional density around the centers of the channels, whose values hardly depend on the $z$ coordinate (Fig. 2). This indicated the presence of indium at the centers of the channels. The continuous character of the density along **c** indicated that the positions of the In atoms in different channels are not correlated, in agreement with the results of Boswell & Bennet (1996). The indium substructure was described by the two twofold special positions (0,0,0) and (0,0,$\frac{1}{4}$), which were partially occupied by In atoms for a fraction $x$. Subsequent refinements varied all atomic coordinates as allowed by symmetry, an isotropic temperature parameter for each independent atom and the occupancies of both indium sites (that were constrained to be equal). A smooth convergence towards $R_p = 0.026$ and $R_{Bragg} = 0.043$ was obtained. In the final refinement the parameters of the profile and background functions as well as the lattice parameters were also varied (Fig. 3). The final results are summarized in Table 1.[1] All refinements were performed with the computer program *JANA*2000 (Dušek *et al.*, 2001). The apparent composition $x$ = 0.539 (4) is different from the nominal composition $x_n = 0.75$. However, the uncertainty on the position of indium in the direction along the channels as well as the expected correlations between $x$ and the temperature factor imply that the apparent composition is not necessarily the true composition of $In_xNb_3Te_4$. On the other hand, the true composition is not equal to the nominal composition either, because of impurity phases and possible losses of indium due to reaction with the quartz tube. An attempt to determine the exact indium composition *via* energy dispersive X-ray microanalysis (EDX) was not successful. Indium was found by this technique, but the observed values for In:Nb:Te varied from 0.80:3:4.95 to 1.06:3:5.27. The good fit in the Rietveld refinement of the high-energy X-ray data showed that the Nb:Te ratio is very close to 3:4. The large variations in the EDX results, and the differences between compositions obtained by X-rays and EDX might be caused by inhomogeneities of the sample and the surface sensitivity of EDX. This surface is formed by the surfaces of the individual powder grains. The method used to prepare the sample, *i.e.* the reaction of indium metal with $Nb_3Te_4$ powder, might have led to the formation of In–Nb–Te impurity phases which are specifically located at the surfaces of the grains. The X-ray scattering indicates less than 5% impurity phases, but EDX has

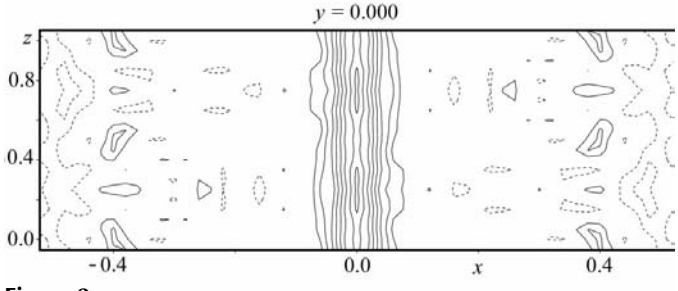


**Figure 2**
The (010) section of the difference Fourier of $In_xNb_3Te_4$ ($x$ = 0.54) based on a refinement without In atoms. Contours of constant positive density are drawn at intervals of 1.5 e Å$^{-3}$. Negative density is represented by dotted contours at intervals of 1.5 e Å$^{-3}$. Density at the centers of the channels clearly show the positions of In.

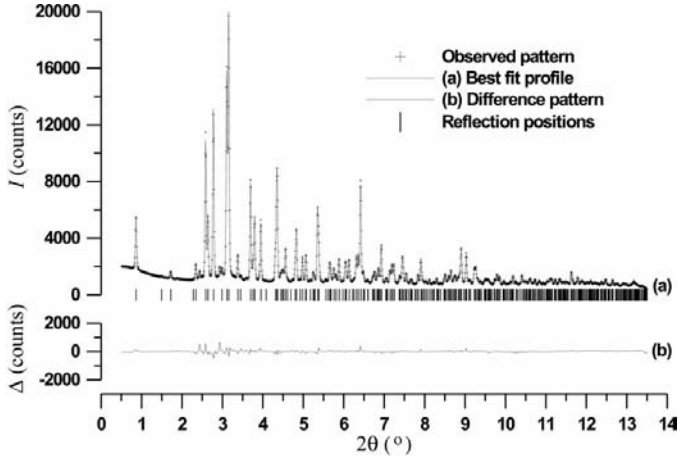


**Figure 3**
Best-fit profile of the Rietveld refinement of $In_xNb_3Te_4$ ($x$ = 0.54) at ambient conditions.

[1] Supplementary data for this paper are available from the IUCr electronic archives (Reference: CK0007). Services for accessing these data are described at the back of the journal.

measured the surface regions which might have been enriched in impurity phases.

The purpose of this high-energy X-ray diffraction experiment was

(i) to show that indium enters into the structure in the channels only, and

(ii) to determine a value for $x$ that could be used and was kept fixed in the high-pressure diffraction studies.

## 3. High-pressure X-ray diffraction

High-pressure X-ray powder diffraction on $Nb_3Te_4$ was measured at beamline ID30 of the ESRF. Similar experiments on $In_xNb_3Te_4$ ($x = 0.54$) were performed at beamline ID9 of the ESRF. For all experiments small amounts of the finely ground samples were loaded into membrane-driven diamond anvil cells (DACs; Letoullec *et al.*, 1988). For each sample two series of experiments were performed. The series with a maximum pressure of ~10 GPa was denoted as the 10 GPa series and the series with a maximum pressure of ~40 GPa was denoted as the 40 GPa series. For the 10 GPa series the DACs was equipped with 600 μm culet diamonds and stainless-steel gaskets with 250 μm diameter holes. A methanol–ethanol mixture was used as the pressure medium. In the 40 GPa series 300 μm culet diamonds, steel gaskets with 125 μm diameter holes and nitrogen as a pressure medium were used. The pressure was determined by the ruby luminescence method using the wavelength shift callibration of Mao *et al.* (1986).

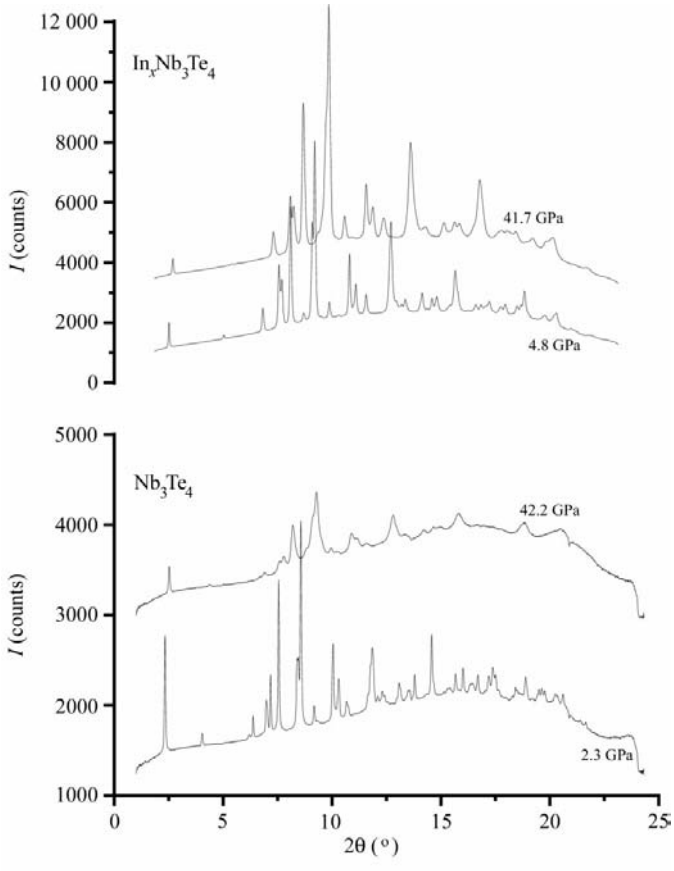


**Figure 4**
X-ray powder diffraction intensity profiles of $Nb_3Te_4$ at pressures of 2.3 and 42.2 GPa and of $In_xNb_3Te_4$ ($x$ = 0.54) at pressures of 4.8 and 41.7 GPa. The intensity as a function of scattering angle was obtained by integration of the powder rings on image plates using the computer program *FIT2D* (Hammersley *et al.*, 1998).

X-ray scattering of $Nb_3Te_4$ powder was measured with monochromatic X-rays of an energy of 33.169 keV ($\lambda = 0.37380$ Å). An online fast-readout image-plate detector was used (Thoms *et al.*, 1998). For the 10 GPa series data were collected at 16 different pressures between 0.13 and 9.95 GPa. Exposure times were between 60 and 120 s. For the 40 GPa series data were collected at 12 different pressures between 2.31 and 42.2 GPa. The exposure time was 39 s for each image.

X-ray scattering of $In_xNb_3Te_4$ powder was measured with monochromatic X-rays of an energy of 28.744 keV ($\lambda = 0.43133$ Å). The X-ray detector was a Marresearch MAR345 online image plate system. The 10 GPa series consisted of images measured at 17 different pressures between 0.26 and 10.82 GPa with exposure times of 9.0 s. The 40 GPa series consists of data collected at 14 different pressures. Owing to difficulties in controlling the pressure, the initial image was measured at 23.35 GPa and the first six images were collected on increasing the pressure from this value to 41.7 GPa. The remaining eight images were collected on decreasing pressure. The final data set was measured at a pressure of 4.84 GPa. Exposure times were between 9 and 40 s.

The data reduction of each image was performed with the computer program *FIT2D* (Hammersley *et al.*, 1998), in a manner analogous to that described above. For each sample and pressure a profile of corrected intensity as a function of the scattering angle was thus obtained.

The quality of the high-pressure data is substantially lower than the quality of the high-energy data. First of all the background is much higher, which can be attributed to scattering of different parts of the DAC. Secondly, the powder rings of maximum intensity on the image plates have a more spotty character than in the high-energy experiment. This can be attributed to the larger amount of exposed sample in the latter experiment. In this respect it is noted that the data quality for $In_xNb_3Te_4$ was better than for $Nb_3Te_4$. We attribute this to $In_xNb_3Te_4$ being a better powder than $Nb_3Te_4$. Finally, it is noted that the high-pressure data could be measured to maximum values for $\sin\theta/\lambda$ of ~0.5 $Å^{-1}$ only, while the high energy data were measured up to $\sin\theta/\lambda = 0.85$ $Å^{-1}$.

Inspection of the intensity profiles showed that neither of the two compounds has a structural phase transition between 0 and 42 GPa (Fig. 4). These observations were confirmed by subsequent structure refinements.

The procedure of analysis was similar for each data set. First a Le Bail-type fit was performed, in order to obtain initial values for the lattice and profile parameters. These parameters were then used in Rietveld refinements of the structures and finally Rietveld refinements were performed, while varying

**Table 3**
Structural parameters of $In_xNb_3Te_4$ ($x$ = 0.54) at selected pressures ($P$).

Nb is at ($x$, $y$, $\frac{1}{4}$), Te1 is at (2/3, 1/3, $\frac{1}{4}$), Te2 is at ($x$, $y$, $\frac{1}{4}$), In1 is at (0, 0, 0) and In2 is at (0, 0, $\frac{1}{4}$).

| Parameter | $P$ = 0.5 GPa | $P$ = 29.6 GPa |
|---|---|---|
| $a$ (Å) | 10.6599 (2) | 9.9576 (9) |
| $c$ (Å) | 3.6533 (1) | 3.4264 (3) |
| $x$(Nb) | 0.4872 (4) | 0.4879 (5) |
| $y$(Nb) | 0.0996 (4) | 0.1063 (5) |
| $U_{iso}$(Nb) | 0.0226 (8) | 0.022 (1) |
| $x$(Te2) | 0.3357 (4) | 0.3186 (5) |
| $y$(Te2) | 0.2724 (3) | 0.2583 (4) |
| $U_{iso}$(Te) | 0.0226 (8) | 0.034 (1) |
| $U_{iso}$(In) | 0.065 (9) | 0.03 (1) |

structural as well as profile and lattice parameters. The almost symmetrical peak profiles were adequately described by pseudo-Voigt functions and an empirical asymmetry correction. A manual background was used.

The inferior quality of the high-pressure data forced us to impose additional restrictions on the parameters compared with the high-energy data set of $In_xNb_3Te_4$. A severe correlation was observed between lattice parameters, zero-shift along $2\theta$ and the asymmetry parameter of the profile. Therefore, these parameters were only refined for the lowest pressure data within each series, while the zero-shift and the asymmetry parameter were kept at these values for all other refinements within the same series. Although there might still be a rather large error in the absolute values of the lattice parameters, this procedure ensures that within each series relative values are accurate and thus reliable values for the compressibilities will be obtained. The zero-shifts were introduced to account for small inaccuracies of the position of the beam center and of the step width in $2\theta$. For $In_xNb_3Te_4$ the occupancies of the In sites were fixed at their values obtained from the high-energy X-ray data (occupancy = $x/2$ = 0.27), but individual isotropic temperature factors could be used. For $Nb_3Te_4$ it appeared necessary to use one isotropic temperature factor for all three independent atoms. Finally it appeared to be necessary to include the effects of preferred orientation. The March model was used with one parameter describing the degree of preferred orientation of needles with fibre axis ⟨001⟩.

Rietveld plots of typical refinements are presented in Fig. 5 for $Nb_3Te_4$ at 0.4 GPa and in Fig. 6 for $In_xNb_3Te_4$ at 29.6 GPa. The variations in data quality lead to a spread in accuracies of the refined parameters, as can be seen in Tables 2 and 3.

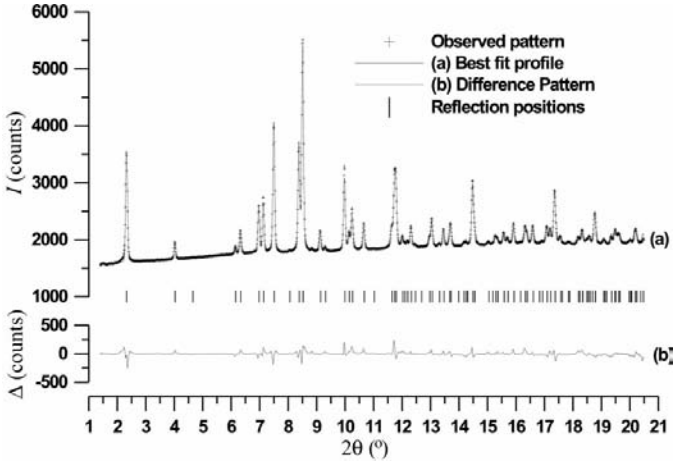


**Figure 5**
Best-fit profile of the Rietveld refinement of $Nb_3Te_4$ at 0.4 GPa pressure.

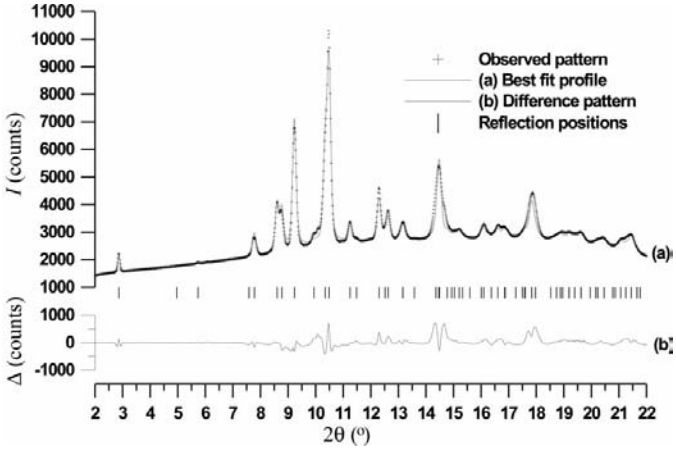


**Figure 6**
Best-fit profile of the Rietveld refinement of $In_xNb_3Te_4$ ($x$ = 0.54) at 29.6 GPa pressure.

## 4. Discussion

We have obtained complete structural information on the two compounds $Nb_3Te_4$ and $In_xNb_3Te_4$ [$x$ = 0.539 (4)] at a series of

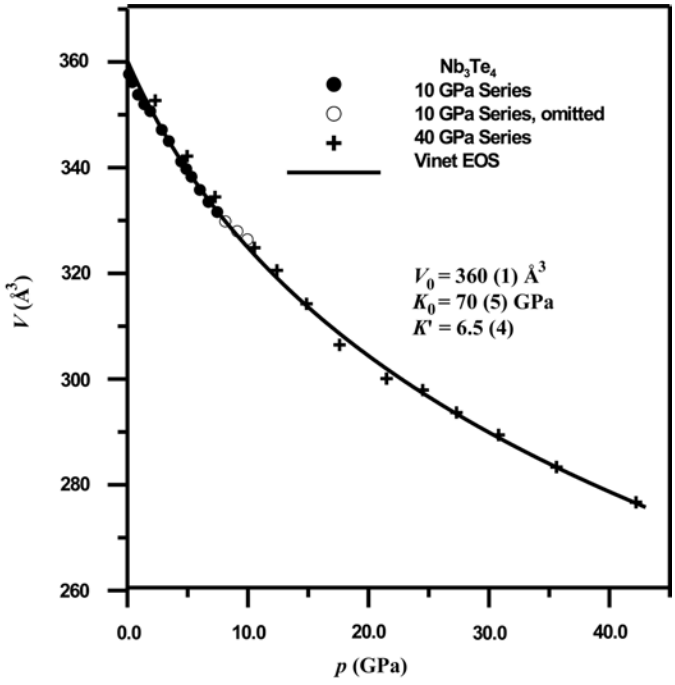


**Figure 7**
Pressure dependence of the unit cell volume of $Nb_3Te_4$.

pressures between 0 and 40 GPa. The first type of information that can be derived from these data is the pressure dependence of the volume of the unit cell. This relation defines the room-temperature section of the thermodynamic equation-of-state (EOS).

For both compounds a good fit to the data was obtained with a Vinet-type EOS

$$P = 3K_0[(1 - f_V)/f_V^2]\exp\left[\tfrac{3}{2}(K' - 1)(1 - f_V)\right] \qquad (1)$$

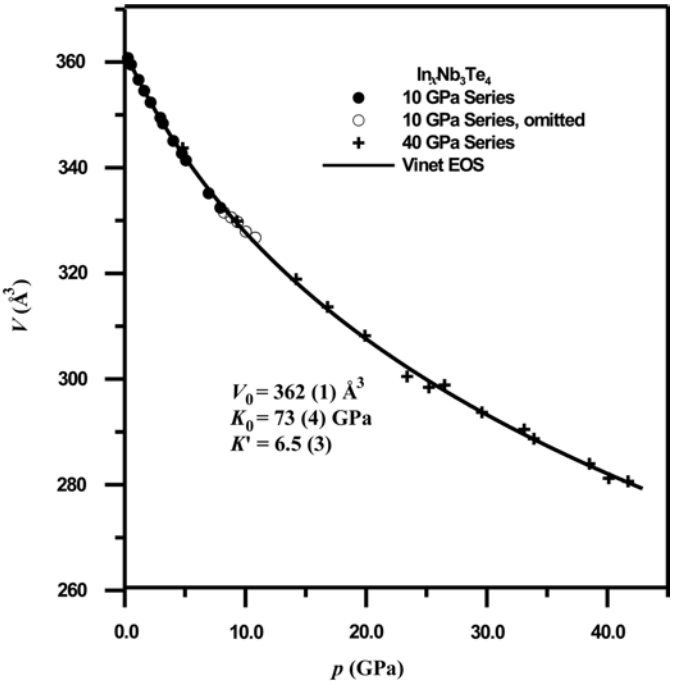


**Figure 8**
Pressure dependence of the unit-cell volume of $In_xNb_3Te_4$ ($x$ = 0.54).

using the computer program *EOSFIT* by Angel (2000). $f_V$ is defined as $f_V = (V/V_0)^{1/3}$. In this way the bulk modulus ($K_0$) and unit-cell volume ($V_0$) at zero pressure as well as the pressure derivative of the bulk modulus $K'$ were determined (Figs. 7 and 8). For both 10 GPa series the data shows an upturn for pressures above 8 GPa, which is not continued in the 40 GPa series. We attribute this upturn to freezing the pressure-transmitting medium and the resulting non-hydrostatic conditions. These points were excluded from the fits. A slight mismatch between data from the two series is visible for $Nb_3Te_4$. We attribute this to problems with the correlations between lattice parameters and zero shifts in the refinements in combination with the uncertainty of the absolute value of the pressure, due to the strong temperature dependence of the wavelength of the ruby luminescence. The most striking result is that the compressibilities of $Nb_3Te_4$ and $In_xNb_3Te_4$ are equal, despite the higher density of the latter compound.

The linear compressibilities along and perpendicular to the hexagonal axes are obtained from the pressure dependences of the lattice parameters $c$ and $a$ (Figs. 9 and 10). From these results follows that the compressibilities are anisotropic with the larger compression in the direction perpendicular to the hexagonal axis. It should be noted that the refinements exhibited quite large correlations between the $a$ and $c$ lattice parameters, such that the individual values are much less accurate than the volume of the unit cell.

The results of the Rietveld refinements allow the analysis of the pressure dependence of the characteristic structural features. It is noted that in a compound with a perfectly isotropic and homogeneous compression behaviour, the relative changes of the interatomic distances are equal to the linear compressibility and bond angles do not change values. For an anisotropic compressibility, but otherwise homo-

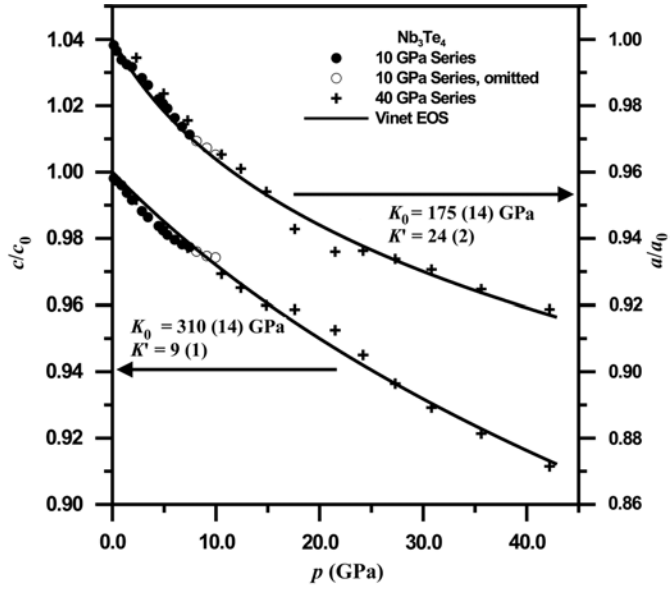


**Figure 9**
Pressure dependence of the relative compression along the $a$ axis (upper trace, right scale) and along the hexagonal $c$ axis (lower trace, left scale) of $Nb_3Te_4$.

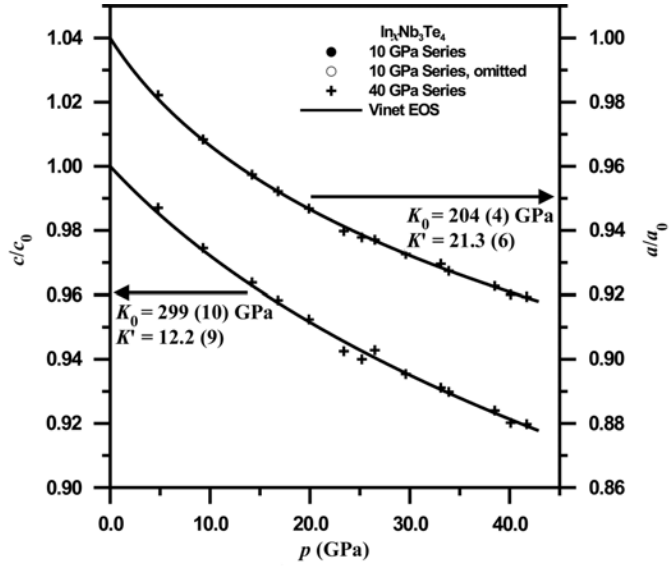


**Figure 10**
Pressure dependence of the relative compression along the $a$ axis (upper trace, right scale) and along the hexagonal $c$ axis (left scale) of $In_xNb_3Te_4$ ($x$ = 0.54).

geneous compression behaviour the relative change of a bond length will depend on the orientation of this bond with respect to the lattice. Here we will show that the compressions of $Nb_3Te_4$ and $In_xNb_3Te_4$ are neither isotropic nor homogeneous.

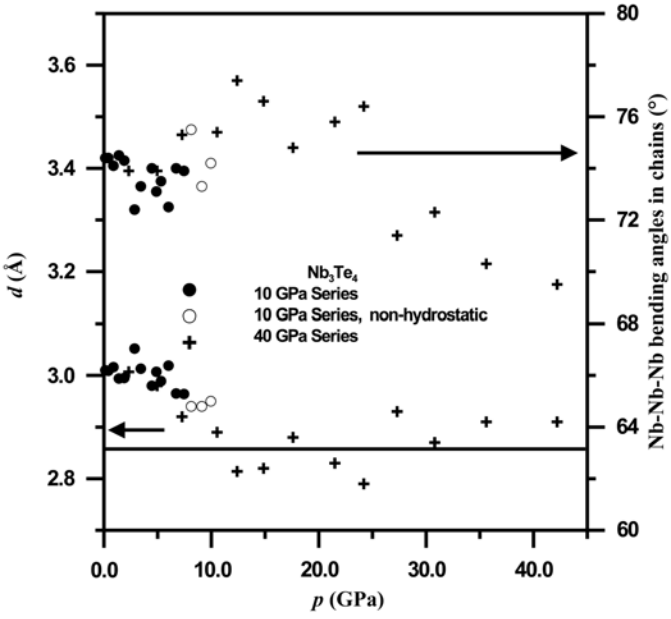


**Figure 11**
Pressure dependence of the niobium–niobium distance (lower trace, left scale) and the bending angles (upper trace, right scale) of the niobium zigzag chains of $Nb_3Te_4$. The line represents the metallic Nb—Nb distance at ambient conditions.

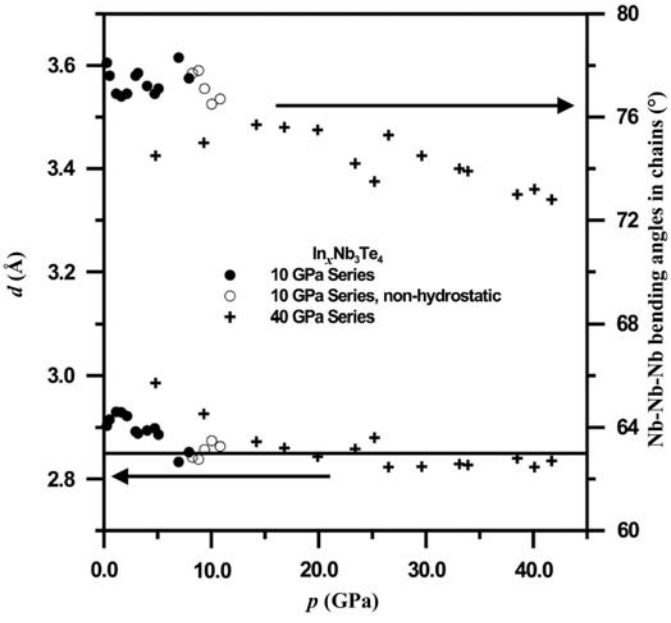


**Figure 12**
Pressure dependence of the niobium–niobium distance (lower trace, left scale) and the bending angles (upper trace, right scale) of the niobium zigzag chains of $In_xNb_3Te_4$ ($x$ = 0.54). The line represents the metallic Nb—Nb distance at ambient conditions.

First, consider the shortest Nb—Nb distance, with values of $d_1 = 3.010$ (6) Å in $Nb_3Te_4$ and $d_2 = 2.903$ (5) Å in $In_xNb_3Te_4$ at the lowest pressures. The pressure dependence of these distances show that they decrease by ~0.1 Å up to pressures of 10 GPa for $Nb_3Te_4$ and 8 GPa for $In_xNb_3Te_4$ (Figs. 11 and 12). Beyond 10 GPa they hardly change any more. In both compounds the high-pressure values of these distances are near the value of 2.86 Å for the Nb—Nb distance in niobium metal at ambient pressure (Villars & Calvert, 1996). The origin of the relatively large scatter of the data points of $Nb_3Te_4$ around a smooth curve is not understood, but obviously it represents the uncertainty for the positions of the Nb atoms. The mismatch between the data from the 10 GPa series and the 40 GPa series of $In_xNb_3Te_4$ might be related to the phase transition at $p = 16.3$ GPa of the pressure-transmitting medium nitrogen (Olijnyk, 1990). The fact that the outlier points at 4.8 and 9.3 GPa were obtained on releasing the pressure might then be responsible for non-hydrostatic conditions below 16.3 GPa.

The shortest Nb—Nb distance occurs between Nb atoms with $z$ coordinates fixed at 0.25 and 0.75, respectively. As the **c** axes continue to decrease up to the highest pressures {[$c$(10 GPa) − $c$(40 GPa)]/2 = 0.1055 Å}, but the Nb—Nb distances are virtually constant above 10 GPa, the Nb atoms on neighbouring mirror planes must move in different directions in the plane. The relative coordinates of these atoms change (Tables 2 and 3), and the compression is inhomogeneous. The zigzag Nb chains are folded up on increasing pressure, without changing the length of the individual sections (Figs. 11 and 12).

The second feature of interest is the diameter of the channel. The radius of the channel is defined as the distance between its axis at $(0,0,\frac{1}{4})$ and the bounding tellurium Te2 at $(x,y,\frac{1}{4})$ (Tables 2 and 3). The pressure dependences of the channel radii in the two compounds produce smooth curves (Figs. 13 and 14). They can be fitted with a Vinet EOS and they result in an apparent bulk modulus that is equal to the values obtained from the cell volume. A comparison of the pressure dependences of the radius of the channels and the $a$ lattice parameters shows that all the compression along the $a$ direction results from a compression of the channels (Figs. 13 and 14). A highly inhomogeneous compression behaviour is thus found. The initially surprising result is that the compression of empty channels in $Nb_3Te_4$ and partially filled channels in $In_xNb_3Te_4$ is similar. An explanation is that the radius of the channels (between 2.85 and 3.3 Å) is larger than the equilibrium In—Te distance (2.82 Å at ambient conditions; Villars & Calvert, 1996). Differences of the compressibilities between $Nb_3Te_4$ and $In_xNb_3Te_4$ can thus be expected for pressures that are substantially higher than 40 GPa.

## 5. Conclusions

The structures of $Nb_3Te_4$ and $In_xNb_3Te_4$ [$x$ = 0.539 (4)] have been determined as a function of pressure between 0 and 40 GPa. It is shown that the compression is inhomogeneous. Perpendicular to the hexagonal axes it involves the compres-

sion of the channels in these compounds. Along the hexagonal axes the zigzag niobium chains are folded rather than Nb—Nb distances becoming shorter. The bonding angle of the zigzag chains thus decreases, and a substantial influence of pressure on the electronic properties can be expected.

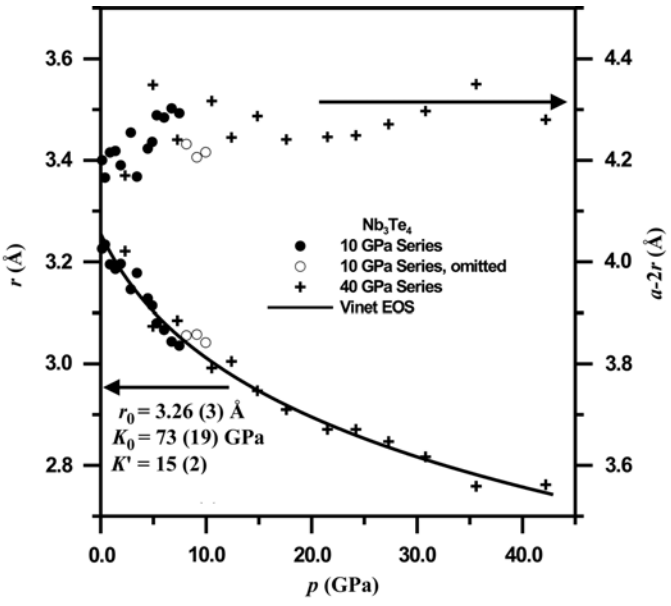


**Figure 13**
Pressure dependence of the radius ($r$) of the hexagonal channels of $Nb_3Te_4$ (lower trace, left scale) and of $a$–$2r$ (upper trace, right scale) to illustrate that the compression along **a** is due to compression of the channels.

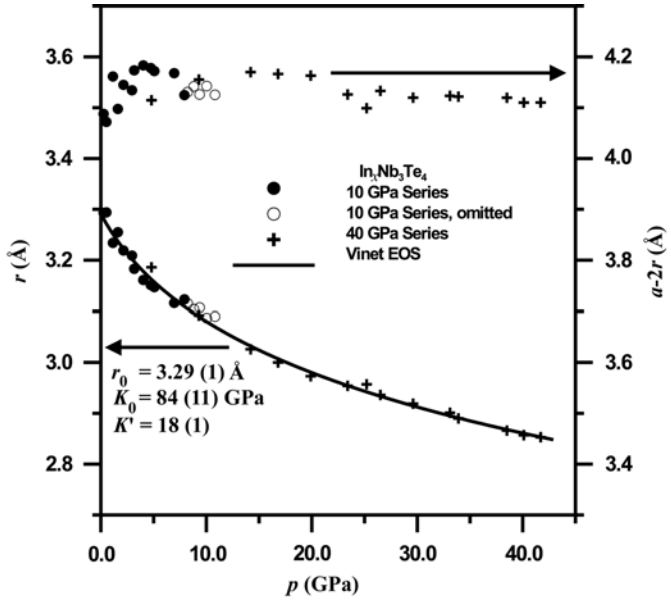


**Figure 14**
Pressure dependence of the radius ($r$) of the hexagonal channels of $In_xNb_3Te_4$ ($x = 0.54$; lower trace, left scale) and of $a$–$2r$ (upper trace, right scale) to illustrate that the compression along **a** is due to compression of the channels.

The most striking result is that the compression behaviour of $Nb_3Te_4$ and $In_xNb_3Te_4$ is found to be nearly equal. Although an explanation was provided by the observation that the In atoms are of smaller size than the diameter of the channels, it is still noteworthy that the disorder and thermal vibrations of In hardly influence the compression behaviour.

The bulk modulus was found as $K_0 = 70\,(5)$ GPa for $Nb_3Te_4$ and $K_0 = 73\,(4)$ GPa for $In_xNb_3Te_4$. These values imply a relatively soft material as compared with, for example, $NbSe_2$ ($K_0 = 125$ GPa) or $TaSe_2$ ($K_0 = 148$ GPa) or pure niobium ($K_0 = 170$ GPa) or tantalum ($K_0 = 191$ GPa) (Landolt & Börnstein, 1992).

We are grateful to Michael Hanfland (beamline ID9, ESRF) and the staff of beamline ID15B (ESRF) for their help with the X-ray scattering experiments. Beamtime at the European Synchrotron Radiation Facility (ESRF) was obtained under the proposal No. HS1094. We also thank Johannes Etzkorn and Professor Dr Harald Hillebrecht (Inorganic Chemistry I, University of Bayreuth) for the EDX measurements. Financial support by the Deutsche Forschungsgemeinschaft (DFG) and the VCI is gratefully acknowledged.

## References

Angel, R. J. (2000). *Berichte aus den Arbeitskreisen der DGK*, edited by R. E. Dinnebier, Vol. 9, pp. 209–229. Kiel: Deutsche Gesellschaft für Kristallographie.
Boswell, F. W. & Bennet, J. C. (1996). *Mater. Res. Bull.* **31**, 1083–1092.
Dušek, M., Petříček, V., Wunschel, M., Dinnebier, R. E. & van Smaalen, S. (2001). *J. Appl. Cryst.* **34**, 398–404.
Hammersley, A. P., Svensson, S. O., Hanfland, M., Fitch, A. N. & Hausermann, D. (1998). *High Press. Res.* **14**, 235–248.
Huan, G. & Greenblatt, M. (1987). *Mater. Res. Bull.* **22**, 943–949.
Ishihara, Y. & Nakada, I. (1982). *Solid State Commun.* **42**, 579–582.
Ishihara, Y. & Nakada, I. (1983). *Solid State Commun.* **45**, 129–132.
Landolt, H. & Börnstein, R. (1992). *Numerical Data and Functional Relationships in Science and Technology/New Series*, edited by D. F. Nelson, Vol. III/29/a. Berlin: Springer.
Letoullec, R., Pinceaux, J. P. & Loubeyre, P. (1988). *High Press. Res.* **1**, 77–90.
Mao, H. K., Xu, J. & Bell, P. M. (1986). *J. Geophys. Res.* **91**, 4673–4676.
Olijnyk, H. (1990). *J. Chem. Phys.* **93**, 8968–8972.
Oshiyama, A. (1983). *J. Phys. Soc. Jpn*, **52**, 587–596.
Othani, T., Sano, Y. & Yokota, Y. (1993). *J. Solid State Chem.* **103**, 504–513.
Othani, T., Yokota, Y. & Sawada, H. (1999). *Jpn. J. Appl. Phys.* **38**, L142–L144.
Sekine, T., Kiuchi, Y., Matsuura, E., Uchinokura, K. & Yoshizaki, R. (1987). *Phys. Rev. B*, **36**, 3153–3160.
Selte, K. & Kjekshus, A. (1964). *Acta Cryst.* **17**, 1568–1572.
Suortti, P., Buslaps, T., Honkimäki, V., Kretzschmer, M., Renier, W. & Shukla, A. (2001). Submitted.
Thoms, M., Bauchau, S., Hausermann, D., Kunz, M., Le Bihan, T., Mezouar, M. & Strawbridge, D., (1998). *Nucl. Instrum. Methods Phys. Res. A*, **413**, 175–184.
Villars, P. & Calvert, L. D. (1996). *Pearson's Handbook of Crystallographic Data for Intermetallic Phases*, 2nd ed. Materials Park, Ohio: ASM International.